Article type : Original Article

Variations in magmatism and the state of tectonic compensation of the Mariana subduction system

Hongyu Li[1], Jian Lin[1,2,4,5*], Zhiyuan Zhou[2,3*], Fan Zhang[2,3], Laiyin Guo[5]

[1] *State Key Laboratory of Marine Geology, School of Ocean and Earth Science, Tongji University, Shanghai 200092, China*

[2] *Key Laboratory of Ocean and Marginal Sea Geology, South China Sea Institute of Oceanology, Innovation Academy of South China Sea Ecology and Environmental Engineering, Chinese Academy of Science, Guangzhou 510301, China*

[3] *Southern Marine Science and Engineering Guangdong Laboratory, Guangzhou 511458, China*

[4] *Department of Geology and Geophysics, Woods Hole Oceanographic Institution, Woods Hole, MA 02543, USA*

[5] *Department of Ocean Science and Engineering, Southern University of Science and Technology, Shenzhen 518055, China*

Corresponding authors:

Jian Lin (jlin@whoi.edu), ORCID: https://orcid.org/0000-0002-6831-2014

Zhiyuan Zhou (zyzhou@scsio.ac.cn), ORCID: https://orcid.org/0000-0002-8963-3167

Running head: Tectonic compensation of the Mariana subduction zone

Statement of significance

The Mariana subduction zone has experienced multi-stage arc rifting and magma accretion. Remarkable variations in crustal thickness and the state of tectonic compensation are found along the Mariana Trench, Mariana Arc, Mariana Trough, and West Mariana Ridge. The positive isostatic anomalies in the southern Mariana Arc at 12.5°–16.7°N can be explained by two possibilities: (1) Late-stage magma accretion on a relatively strong lithosphere in the southern Mariana Arc; (2) Tectonic stresses transmitted through the coupling interface between the lower and upper plates. These findings advance our understanding of the tectonic processes of this classic arc-trench system.

Abstract

We investigate the variations in the state of isostatic compensation of the Mariana subduction system. We first calculate and analyze the gravity-derived crustal thickness and non-isostatic topography of this region. The Mariana back-arc spreading center and West Mariana Ridge are both close to Airy isostatic compensation. In contrast, the Mariana Trench axis is associated with a clearly defined zone of negative non-isostatic topography and free-air gravity anomaly, which have been shown to be caused by the flexural bending of the subducting Pacific Plate. The new analyses reveal that the southern Mariana Arc at 12.5°–16.7°N is associated with positive non-isostatic topography and a free-air gravity anomaly, which we interpret to be the result of accretion of young volcanism on a relatively strong lithospheric plate and/or supported by the tectonic stresses induced by the interaction of the subducting Pacific Plate with the upper Mariana micro-plate.

1 | INTRODUCTION

The Mariana is an intra-oceanic convergent margin in the western Pacific Ocean, where the oldest oceanic plate on Earth currently subducts. The Mariana subduction system, from east to west, consists of the Mariana Trench, Mariana Arc, Mariana Trough, West Mariana Ridge, Parece Vela Basin, and Palau-Kyushu Ridge (Figure 1). The Challenger Deep, the deepest point on the Earth's surface, is located at the southern end of the Mariana Trench.

The subduction of this region initiated in the early Eocene (~50 Ma). The first arc began to form at ~40 Ma and continued up to ~30 Ma (Fryer, 1996; Hussong & Uyeda, 1981; Stern & Bloomer, 1992; Cosca et al., 1998; Ishizuka et al., 2018; Reagan et al., 2019). The first arc then rifted longitudinally to form the Palau-Kyushu Ridge. Subsequently, back-arc spreading began and the Palau-Kyushu Ridge moved away from the trench, creating the Parece Vela

Basin (Taylor 1992). Owing to the continued magma supply, a second arc was established at ~15 Ma on the eastern half of the original arc. The second arc split longitudinally again at ~8 Ma and the West Mariana Ridge formed (Seama & Fujiwara, 1993). Seafloor spreading began at ~4 Ma and persists to date, forming the Mariana Trough (Bibee et al., 1980; Yamazaki & Stern, 1997; Stern et al., 2003). Magma upwelling continued at the eastern half of the second arc, and the Mariana Arc formed.

The unusually high topography in the southern Mariana Arc has been discussed in previous studies (Gvirtzman & Stern, 2004; Chapp et al., 2008). It was proposed that the deflections of the Earth's surface and the lateral variations in mantle density at convergent margins are mainly controlled by the properties of the sinking slab and the surrounding mantle (Isacks et al., 1968). The multiple rifts of the Mariana Arc complicated the morphology and isostatic state in this region. The causes of observed anomalies in topography and isostasy remain poorly known.

In this study, we first calculate the gravity-derived crustal thickness and non-isostatic topography of this region using bathymetry, sediment thickness, crustal age, and gravity data. We then investigate the state of tectonic compensation of the key tectonic provinces of the Mariana system. We analyze the variations along the Mariana Trench, Mariana Arc, Mariana Spreading Center, and West Mariana Ridge in terms of their topography, crustal thickness, and non-isostatic topography. We also analyze the remarkably different geological characteristics of the northern and southern parts of this system. We propose that the late-stage magma accretion on a relatively thick and strong lithospheric plate may cause the positive anomalies in the morphology and non-isostatic topography of the southern Mariana Arc. The interaction between the lower and upper plates could also provide additional lithospheric stresses to support the excess mass in the southern Mariana Arc.

2 | DATA AND METHODS

2.1 | Data

The bathymetry data are obtained from the global bathymetry and topography dataset (SRTM15+V2.1; Tozer et al., 2019) at a resolution of 15 arc seconds (Figure 1). The free-air gravity anomaly (FAA) is extracted from the global gravity anomaly dataset (V30.1; Sandwell et al., 2014) at 1-arc-minute grid (Figure 2a). We obtain the sediment thickness from the 5-arc-minute global database of Straume et al. (2019) (Figure S1a). The crustal age data of 6-arc-minute is obtained from the global dataset of Müller et al. (2019). We interpolate the crustal age data to illuminate the tectonic history of the Mariana subduction system (Hussong & Uyeda, 1981; Stern & Bloomer, 1992).

2.2 | Mantle Bouguer and residual mantle Bouguer gravity anomalies

Following the method of Parker (1973), the gravitational effects of the water–sediment, sediment–crust, and crust–mantle interfaces are calculated and removed from the FAA to obtain the mantle Bouguer gravity anomaly (MBA), with a reference crustal thickness of 6 km (Figure 2b). The densities of water, crust, and mantle are assumed to be 1.03, 2.7, and 3.3×10^3 kg/m^3, respectively (Table 1). The gravitational effects of the descending slab, which are not included in this study, are limited to regions near the trench axis (Watts & Talwani, 1975; Martinez et al., 2018).

Thermal correction is performed by removing the gravitational effect of 1D lithospheric cooling (Figure S1b) from the MBA to obtain the residual mantle Bouguer gravity anomaly (RMBA, Figure S1c). The gravitational effect of the lithospheric cooling is calculated based on a plate cooling model, assuming the plate thickness to be 100 km (Turcotte & Schubert, 2014). The temperatures of the upper and lower boundaries of the plate are set to $T_0 = 0$ °C and $T_1 = 1{,}350$ °C, respectively. The density anomaly of the mantle lithosphere is defined by $\Delta\rho= \alpha(T_1–T)\rho_{m0}$, where ρ_{m0} and α are the reference mantle density (3.3×10^3 kg/m^3) and thermal expansion coefficient (3×10^{-5} K^{-1}), respectively (Table 1).

2.3 | Crustal thickness and non-isostatic topography

The variations in crustal thickness, as well as crustal and mantle densities all contribute to the RMBA (Canales et al., 2002). Here we examine an end-member model in which the main contribution to the RMBA is the variation in crustal thickness (Kuo & Forsyth, 1988; Lin et al., 1990; Wang et al., 2011). The crustal thickness is calculated by downward continuation of the RMBA to a reference depth and then calibrated using available seismic data (Takahashi et al., 2007; Wan et al., 2019).

The Airy isostatic topography of the study area is calculated based on the model of local Airy isostatic compensation: $T_{iso}=(H_c–H_0)\times(\rho_{m0}–\rho_c)/(\rho_{m0}–\rho_w)$, where H_c is the gravity-derived crustal thickness and H_0 is the reference oceanic crustal thickness; ρ_w and ρ_c are the water and crustal densities, respectively (Table 1). Thermal subsidence of the lithosphere is estimated using a 1D plate-cooling model (Turcotte & Schubert, 2014). Non-isostatic topography ($T_{non-iso}$) is calculated by subtracting the effects of sediment loading (T_{sed}), thermal subsidence ($T_{thermal}$), and the Airy isostatic topography (T_{iso}) from the observed topography: $T_{non\text{-}iso}=T_{topo}-T_{sed}-T_{iso}+T_{thermal}$. This calculation method is described in Zhang et al. (2014).

3 | RESULTS

3.1 | Topography and crustal thickness

The seafloor of the northern Mariana Trough (north of 14°N) is characterized by faulted blocks and deep grabens (Figure 1). The presence of an axial valley in the northern Mariana Trough, together with the rugged topography, indicate relatively low magma supply in this region. In contrast, the southern Mariana Trough (south of 14°N) is less rough in morphology and has an axial high at the spreading center, implying enhanced magma supply. It has been proposed that such an increase in magma supply could be due to the southern extension of the spreading center, capturing the hydrous melts above the subducting slab (Martinez et al., 2018). The gravity-derived crustal thickness along the Mariana Spreading Center varies significantly and is less than 2 km at ~20°N (Figures 3a and 4b). Our results are consistent with the gravity analysis of Kitada et al. (2006).

The gravity-derived crustal thickness of the entire Mariana Arc varies slightly, with an average value of ~16 km (Figures 3a and 4c). The southern segment of the Mariana Arc (12.5°–16.7°N) is apparently associated with relatively high topography. However, the crustal "root" is absent in the southern Mariana Arc. The crustal thickness of the West Mariana Ridge decreases south of 15°N (Figures 2b), with an average value of ~13 km (Figure 4a). The crustal thickness along the Mariana Trench is associated with local topographic variations (Figure 4d).

3.2 | Free-air gravity anomalies and non-isostatic topography

The Mariana Spreading Center and West Mariana Ridge are close to local Airy isostasy (Figures 3b and 5), as the elevated seafloor is in general compensated by crustal "roots", except for the short-wavelength features. The means of the non-isostatic topography of the Mariana Spreading Center and West Mariana Ridge are 0.16 km and 0.71 km, respectively, with relatively small standard deviations (STD). In contrast, the bending of the Mariana Trench leads to significant negative isostatic anomalies (Figures 3b and 4d). The Mariana Trench depth is the greatest in the southernmost segment, indicating stronger flexural bending near the Challenger Deep (Zhang et al., 2014; Zhou & Lin, 2018). The mean and STD of the non-isostatic topography of the Mariana Trench are -2.36 km and 1 km, respectively (Figure 5). The southern Mariana Arc appears to deviate significantly from Airy isostasy, with positive isostatic anomalies at 12.5°–16.7°N (Figures 3b and 4c). The mean and STD of the non-isostatic topography of the Mariana Arc are 1.16 km and 1.2 km, respectively (Figure 5).

4 | DISCUSSION

The Mariana forearc formed during the initiation of the subduction system in this region, at ~50 Ma. (Stern & Bloomer, 1992; Ishizuka et al., 2018). The age of the upper plate between the Palau-Kyushu Ridge and Mariana Trench is <50 Ma. Here, the gravity-derived oceanic crustal thickness is constrained and compared with seismic data (Figure S2, Takahashi et al., 2007; Wan et al., 2019). The overall patterns are consistent between the seismically determined and gravity-derived crustal thickness for the overriding plate.

Gvirtzman & Stern (2004) assumed the Mariana Arc to be in a state of isostasy in spite of the high positive FAA in its southern segment. To confirm the observed isostatic anomalies in the southern Mariana Arc, we assume a reference crustal thickness of 6 km and estimated the Moho depth in the study area based on the topography and local Airy isostatic compensation. We then calculate the total gravitational effects of the topography and Moho depth. (Figure S3a). We subtract these gravitational effects from the FAA to obtain the residual gravity anomalies, which reflect non-isostatic compensation and density variations (Figure S3b). Positive anomalies are still obvious in the southern Mariana Arc, as indicated in Figure S3b. This result implies the presence of tectonic stresses in the upper plate, which could maintain the excess mass. Below we present two mechanisms that could explain these topographic and isostatic anomalies.

4.1 | Magma accretion on a relatively strong plate

The Mariana Arc has experienced multiple stages of rifting and magma accretion. Magma accretion on a relatively old and strong plate, which is yet to reach isostatic equilibrium, can explain the observed positive anomalies in topography, non-isostatic topography, and the FAA in the southern Mariana Arc. Within a single subduction system, arcs may rift at different axes during different time periods (Oakley et al., 2009). Profiles of topography, non-isostatic topography, and gravity-derived Moho depths at 19°N and 13.6°N (Figures 6 and 7) illustrate arc rifting processes. The distinct scarps shown in topography (Figure 1) and the thin crust in the northern Palau-Kyushu Ridge reveal that the first arc ruptured along the western side of arc axis in the north (Oakley et al., 2009), leaving most of its volume on the eastern portion (Figures 6a and 7a). The second arc rifted along the eastern side of arc axis north of 15°N (Figures 6a and 7c) and along the western side of arc axis south of 15°N (Figures 6b and 7g), as also indicated by the distinct bathymetric scarps in the south and the indistinct boundary between the West Mariana Ridge and Mariana Trough in the north (Oakley et al., 2009). The widening of the northern and central West Mariana Ridge can also indicate that the second arc rifted along the eastern side of arc axis north of 15°N (Figures 1 and 2b). Figures 7d and 7h show that the magma supply continued after rifting. In the north, the magma accreted on the rifted, thus relatively weak arc location. In contrast, the magma intruded into the relatively old and thus stronger arc plate in the south. We propose that the positive isostatic anomaly and FAA at the southern Mariana Arc are due to the magma accretion onto a relatively strong plate. Figure S4 shows the calculated crustal sectional areas of the West Mariana Ridge and Mariana Arc in Table S1. The crustal areas of the West Mariana Ridge decrease southward (Table S1), revealing the different arc splitting axes.

4.2 | Interactions between the overriding and subducting plates

The pinning of the Ogasawara Plateau and Caroline Ridge at the northern and southern ends of the Mariana Trench, respectively, induced a seaward bulging and progressive seaward rollback of the trench axis. At the southern Mariana Trench, the large positive buoyancy of the Caroline Ridge could impede subduction, enlarging the curvature of Mariana Trench and splitting the southern Mariana Arc at 3.7–2.7 Ma (Ribeiro et al., 2013). The Mariana Spreading Center extends to the rifted arc, capturing the hydrous melts above the descending slab, thus enhancing magma supply (Martinez et al., 2000; Ishibashi et al., 2015). As the width of the Mariana forearc narrows southward, the southern Mariana Arc could be in the coupling zone of the lower and upper plates. When the magma rose above the overriding plate, the stresses transmitted through the coupling interface could maintain the elevated topography and isostatic anomalies. The subducting slab imposes forces on the overriding plate, causing the surface deflections in the upper plate (Crameri et al., 2017). The lithospheric stresses are different in the north and south of the Mariana Arc volcanoes (Andikagumi et al., 2020). The forces exerted by the subducting plate on the overriding plate could also support the magma accretion at the southern segment of the Mariana Arc.

5 | CONCLUSIONS

(1) The crustal thickness along the Mariana Spreading Center varies significantly and the thinnest crust is less than 2 km. The crustal thickness of the West Mariana Ridge

decreases slightly southward. The Mariana Arc exhibits slight variations in crustal thickness.

(2) The Mariana Spreading Center and West Mariana Ridge are associated with relatively low value of non-isostatic topography and FAA, and thus are relatively close to Airy isostatic compensation. In contrast, the Mariana Trench is associated with the negative non-isostatic topography and FAA, consistent with a model of flexural bending of the subducting Pacific Plate.

(3) The southern Mariana Arc is associated with relatively positive non-isostatic topography and FAA, consistent with a model of late-stage magma accretion onto a relatively strong lithospheric plate. The positive anomalies in the topography and non-isostatic topography of the southern Mariana Arc can also be attributed to interactions between the lower and upper plates.

ACKNOWLEDGEMENTS

We are grateful to Jasmine Zhu for providing technical assistance and Geodynamics Group at SCSIO for helpful discussions. This study was supported by the Southern Marine Science and Engineering Guangdong Laboratory (Guangzhou, GML2019ZD0205), National Natural Science Foundation of China (41890813, 91628301, 41976064, 41976066, 91858207, and 91958211), Chinese Academy of Sciences (Y4SL021001, QYZDY-SSW-DQC005, and 133244KYSB20180029), Guangdong Basic and Applied Basic Research Foundation (2021A1515012227), China Ocean Mineral Resources Research and Development Association (DY135-S2-1-04), and National Key R&D Program of China (2018YFC0309800 and 2018FY100505).

Data Availability Statement: The data that support the findings of this study are available from the corresponding author upon reasonable request.

REFERENCES

Andikagumi, H., Macpherson, C. G., & McCaffrey, K. J. W. (2020). Upper plate stress controls the distribution of Mariana Arc volcanoes. *Journal of Geophysical Research: Solid Earth*, 125, e2019JB017391. https://doi.org/10.1029/2019JB017391

Bibee, L. D., Shor, G. G., & Lu, R. S. (1980). Inter-arc spreading in the Mariana Trough. *Marine Geology,* 35(1), 183-197. https://doi.org/10.1016/0025-3227(80)90030-4

Bird, P. (2003). An updated digital model of plate boundaries. *Geochemistry, Geophysics, Geosystems*, 4(3). https://doi.org/10.1029/2001gc000252

Crameri, F., Lithgow-Bertelloni, C. R., & Tackley, P. J. (2017). The dynamical control of subduction parameters on surface topography. *Geochemistry, Geophysics, Geosystems*, 18(4), 1661-1687. https://doi.org/10.1002/2017GC006821

Canales, J. P., Ito, G., Detrick, R. S., & Sinton, J. (2002). Crustal thickness along the western Galápagos Spreading Center and the compensation of the Galápagos hotspot swell. *Earth and Planetary Science Letters*, 203(1), 311-327

Cosca, M., Arculus, R., Pearce, J., & Mitchell, J. (1998). ^{40}Ar/ ^{39}Ar and K-Ar geochronological age constraints for the inception and early evolution of the Izu-Bonin-Mariana arc system. *The Island Arc*, 7(3), 579-595. https://doi.org/10.1111/j.1440-1738.1998.00211.x

Chapp, E., Taylor, B., Oakley, A., & Moore, G. F. (2008). A seismic stratigraphic analysis of Mariana forearc basin evolution. *Geochemistry, Geophysics, Geosystems,* 9(10). https://doi.org/10.1029/2008GC001998

Fryer, P. (1996). Evolution of the Mariana convergent plate margin system. *Reviews of Geophysics*, 34(1), 89-125. https://doi.org/10.1029/95RG03476

Gvirtzman, Z., & Stern, R. J. (2004). Bathymetry of Mariana trench-arc system and formation of the Challenger Deep as a consequence of weak plate coupling. *Tectonics*, 23, TC2011. https://doi.org/10.1029/2003TC001581

Hussong, D. M., & Uyeda, S. (1981). Tectonic processes and the history of the Mariana arc: A synthesis of the results of Deep Sea Drilling Project Leg 60. *Initial Reports of the Deep Sea Drilling Project*, 60, 909-929

Isacks, B., Oliver, J., & Sykes, L. R. (1968). Seismology and the new global tectonics. *Journal of Geophysical Research*, 73(18), 5855-5899. https://doi.org/10.1029/JB073i018p05855

Ishibashi, J., Tsunogai, U., Toki, T., Ebina, N., Gamo, T., Sano, Y., . . . Chiba, H. (2015). Chemical composition of hydrothermal fluids in the central and southern Mariana Trough backarc basin. *Deep Sea Research Part II: Topical Studies in Oceanography*, 121, 126-136. https://doi.org/10.1016/j.dsr2.2015.06.003

Ishizuka, O., Hickey-Vargas, R., Arculus, R. J., Yogodzinski, G. M., Savov, I. P., Kusano, Y., . . . Sudo, M. (2018). Age of Izu–Bonin–Mariana arc basement. *Earth and Planetary Science Letters*, 481, 80-90

Kato, T., Beavan, J., Matsushima, T., Kotake, Y., Camacho, J. T., & Nakao, S. (2003). Geodetic evidence of back - arc spreading in the Mariana Trough. *Geophysical Research Letters*, 30(12)

Kitada, K., Seama, N., Yamazaki, T., Nogi, Y., & Suyehiro, K. (2006). Distinct regional differences in crustal thickness along the axis of the Mariana Trough, inferred from gravity anomalies. *Geochemistry, Geophysics, Geosystems*, 7(4). https://doi.org/10.1029/2005GC001119

Kuo, B. Y., & Forsyth, D. W. (1988). Gravity anomalies of the ridge-transform system in the South Atlantic between 31° and 34.5° S: Upwelling centers and variations in crustal thickness. *Marine Geophysical Research*, 10(3-4), 205-232. https://doi.org/10.1007/Bf00310065

Lin, J., Purdy, G. M., Schouten, H., Sempere, J. C., & Zervas, C. (1990). Evidence from gravity data for focused magmatic accretion along the Mid-Atlantic Ridge. *Nature*, 344(6267), 627-632

Martinez, F., Fryer, P., & Becker, N. (2000). Geophysical characteristics of the southern Mariana Trough, 11°50′N–13°40′N. *Journal of Geophysical Research: Solid Earth*, 105(B7), 16591-16607

Martinez, F., Stern, R. J., Kelley, K. A., Ohara, Y., Sleeper, J. D., Ribeiro, J. M., & Brounce, M. (2018). Diffuse extension of the southern Mariana margin. *Journal of Geophysical Research: Solid Earth*, 123(1), 892-916. https://doi:10.1002/2017jb014684

Müller, R. D., Zahirovic, S., Williams, S. E., Cannon, J., Seton, M., Bower, D. J., . . . Liu, S. (2019). A global plate model including lithospheric deformation along major rifts and orogens since the Triassic. *Tectonics*, 38(6), 1884-1907

Oakley, A. J., Taylor, B., Moore, G. F., & Goodliffe, A. (2009). Sedimentary, volcanic, and tectonic processes of the central Mariana Arc: Mariana Trough back-arc basin formation and the West Mariana Ridge. *Geochemistry, Geophysics, Geosystems*, 10(8). https://doi.org/10.1029/2008GC002312

Parker, R. L. (1973). The rapid calculation of potential anomalies. *Geophysical Journal International*, 31(4), 447-455

Reagan, M. K., Heaton, D. E., Schmitz, M. D., Pearce, J. A., Shervais, J. W., & Koppers, A. A. P. (2019). Forearc ages reveal extensive short-lived and rapid seafloor spreading following subduction initiation. *Earth and Planetary Science Letters*, 506, 520-529. https://doi.org/10.1016/j.epsl.2018.11.020

Ribeiro, J. M., Stern, R. J., Martinez, F., Ishizuka, O., Merle, S. G., Kelley, K., . . . Bloomer, S. (2013). Geodynamic evolution of a forearc rift in the southernmost Mariana Arc. *Island Arc*, 22(4), 453-476. https://doi.org/10.1111/iar.12039

Sandwell, D. T., Muller, R. D., Smith, W. H., Garcia, E., & Francis, R. (2014). New global marine gravity model from CryoSat-2 and Jason-1 reveals buried tectonic structure. *Science*, 346(6205), 65-67. https://doi.org/10.1126/science.1258213

Seama, N. & Fujiwara, T. (1993). Geomagnetic anomalies in the Mariana Trough 18° N. *Preliminary Report of the Hakuho-Maru Cruise KH92-1*, 70-71

Stern, R. J., & Bloomer, S. H. (1992). Subduction zone infancy: Examples from the Eocene Izu-Bonin-Mariana and Jurassic California arcs. *Geological Society of America Bulletin*, 104(12), 1621-1636. https://doi.org/10.1130/0016-7606(1992)104<1621:Szieft>2.3.Co;2

Stern, R. J., Fouch, M. J., & Klemperer, S. L. (2003). An overview of the Izu-Bonin-Mariana subduction factory. *Inside of Subduction Factory*, 138, 175-222

Straume, E. O., Gaina, C., Medvedev, S., Hochmuth, K., Gohl, K., Whittaker, J. M., . . . Hopper, J. R. (2019). GlobSed: Updated total sediment thickness in the world's oceans. *Geochemistry, Geophysics, Geosystems*, 20(4), 1756-1772. https://doi.org/10.1029/2018gc008115

Takahashi, N., Kodaira, S., Klemperer, S. L., Tatsumi, Y., Kaneda, Y., & Suyehiro, K. (2007). Crustal structure and evolution of the Mariana intra-oceanic island arc. *Geology*, 35(3), 203-206. https://doi.org/10.1130/G23212a.1

Taylor, B., & Fujioka, K. (1992). Rifting and the volcanic-tectonic evolution of the Izu-Bonin-Mariana arc. In *Proceedings of the Ocean Drilling Program Scientific Results*, 126, 627-651

Tozer, B., Sandwell, D. T., Smith, W. H. F., Olson, C., Beale, J. R., & Wessel, P. (2019). Global bathymetry and topography at 15 arc seconds: SRTM15+, *Earth and Space Science*, 1847-1864. https://doi: 10.1029/2019EA000658

Turcotte, D. L., & Schubert, G. (2014). *Geodynamics Third Edition*. Cambridge University Press.

Wan, K. Y., Lin, J., Xia, S. H., Sun, J. L., Xu, M., Yang, H. F., . . . Xu, H. L. (2019). Deep seismic structure across the southernmost Mariana Trench: Implications for arc rifting and plate hydration. *Journal of Geophysical Research: Solid Earth*, 124(5), 4710-4727. https://doi:10.1029/2018jb017080

Wang, T. T., Lin, J., Tucholke, B., & Chen, Y. J. (2011). Crustal thickness anomalies in the North Atlantic Ocean basin from gravity analysis. *Geochemistry, Geophysics, Geosystems*, 12(3). https://doi.org/10.1029/2010GC003402

Watts, A. B., & Talwani, M. (1975). Gravity effect of downgoing lithospheric slabs beneath island arcs. *Geological Society of America Bulletin*, 86(1), 1-4.

https://doi.org/10.1130/0016-7606(1975)86<1:Geodls>2.0.Co;2

Yamazaki, T., Seama, N., Okino, K., Kitada, K., Joshima, M., Oda, H., & Naka, J. (2003). Spreading process of the northern Mariana Trough: Rifting ‐ spreading transition at 22° N. *Geochemistry, Geophysics, Geosystems*, 4(9)

Yamazaki, T., & Stern, R. J. (1997). Topography and magnetic vector anomalies in the Mariana Trough. *JAMSTEC Journal of Deep Sea Research*, 13, 31-45

Zhang, F., Lin, J., & Zhan, W. H. (2014). Variations in oceanic plate bending along the Mariana trench. *Earth and Planetary Science Letters*, 401, 206-214. https://doi.org/10.1016/j.epsl.2014.05.032

Zhou, Z. Y., & Lin, J. (2018). Elasto-plastic deformation and plate weakening due to normal faulting in the subducting plate along the Mariana Trench. *Tectonophysics*, 734, 59-68. https://doi.org/10.1016/j.tecto.2018.04.008

Figure Captions

Figure 1. Topography of the Mariana subduction system. Double black lines indicate the Mariana Spreading Center, which we identified based on the topography and FAA, as well as from previous studies (Martinez et al., 2000; Bird, 2003; Yamazaki et al., 2003). The Mariana Trench is marked by the white line with triangles.

Figure 2. (a) FAA of the Mariana subduction zone. The isostatic anomaly in the southern Mariana Arc is marked by a red ellipse. (b) MBA of the study region. Symbols are the same as in Figure 1.

Figure 3. (a) Gravity-derived crustal thickness of the study area. (b) Non-isostatic topography of the study area. The positive anomaly of non-isostatic topography in the southern Mariana Arc is marked by a red ellipse. Symbols are the same as in Figure 1.

Figure 4. Profiles of the topography, non-isostatic topography, and gravity-derived Moho depths along the West Mariana Ridge (WMR, a), Mariana Spreading Center (MSC, b), Mariana Arc (MA, c), and Mariana Trench (MTre, d). Non-isostatic topography is shown as red curves. Black curves indicate topography. Blue curves represent basements which were calculated by removing the sediment from the topography. The sediment is thin. The Moho depths are presented by cyan curves. Dotted curves denote areas using interpolated crustal age data in crustal thickness modeling. Profile locations are indicated in Figure 3a. The West Mariana Ridge, Mariana Spreading Center, Mariana Arc, and Mariana Trench are shown as black curves annotated by I, II, III, and IV respectively. The red arrow in panel b indicates the location of the thinnest crust along the Mariana Spreading Center.

Figure 5. The histograms of non-isostatic topography along the Mariana Arc (MA, cyan), West Mariana Ridge (WMR, green), Mariana Spreading Center (MSC, red), and Mariana Trench (MTre, blue).

Figure 6. Cross-sections of topography, non-isostatic topography, and gravity-derived Moho depths along the profiles at 19°N (a) and 13.6°N (b). Symbols are the same as in Figure 4. The black lines annotated by 1 and 2 in Figure 3a indicate the profile locations. From west to east, the geological structures include the Palau-Kyushu Ridge (PKR), Parece Vela Basin (PVB), West Mariana Ridge (WMR), Mariana Trough (MTro), Mariana Arc (MA), and

Mariana Trench (MTre).

Figure 7. Cartons showing the mechanisms causing positive non-isostatic topography in the southern Mariana Arc and the tectonic processes along the profiles at 19°N (a–d) and 13.6°N (e–f), respectively. In the second stage of rifting, the arc rifted along different axes between the northern and southern segments. Magmas continued to upwell on the eastern half of the second arc. Panels d and h show that in the north, the magma rose above the rifted and thus relatively weak arc plate, while in the south, the magma overlay on the relatively old and thus stronger arc plate.

Figure S1. (a) Map of sediment thickness of the study region. (b) The thermal effects of lithospheric cooling based on a plate cooling model. The area between the Palau-Kyushu Ridge and Mariana Trench is less than 50 Ma old. (c) RMBA of the study region. Symbols are the same as in Figure 1.

Figure S2. (a) P-wave velocity model of the central Mariana subduction zone (Takahashi et al., 2007). The black curve represents gravity-derived Moho depth. (b) P-wave velocity profile across the Challenger Deep in the southern Mariana subduction system. The red curve indicates Moho depth constrained by PmP arrivals (Wan et al., 2019). The black curve indicates gravity-derived Moho depth. The locations of the seismic profiles are shown as red lines in Figure S1c.

Figure S3. (a) The total gravitational effects (Δg) of the topography and Moho depth under the assumption of local Airy isostatic compensation. (b) The residual gravity anomalies obtained by removing the Δg from the FAA. The isostatic anomaly is marked by a red ellipse.

Figure S4. Cross-sections of topography, non-isostatic topography, and gravity-derived Moho depths across the West Mariana Ridge (WMR), Mariana Trough (MTro), Mariana Arc (MA), and Mariana Trench (MTre). Symbols are the same as in Figure 4. Calculated crustal areas of the Mariana Arc and West Mariana Ridge are marked as half-transparent green areas. Profile locations are indicated as black lines in Figure S1c.

Table 1 Parameters used in modeling of gravity and isostatic anomalies

Parameter	Definition	Value	Unit

g	Acceleration due to gravity	9.81	m/s^2
ρ_w	Seawater density	1,030	kg/m^3
ρ_c	Crustal density	2,700	kg/m^3
ρ_{m0}	Reference mantle density	3,300	kg/m^3
T_0	Temperature at surface of the plate	0	^oC
T_1	Temperature at bottom of the plate	1,350	^oC
α	Thermal expansion coefficient	3×10^{-5}	K^{-1}

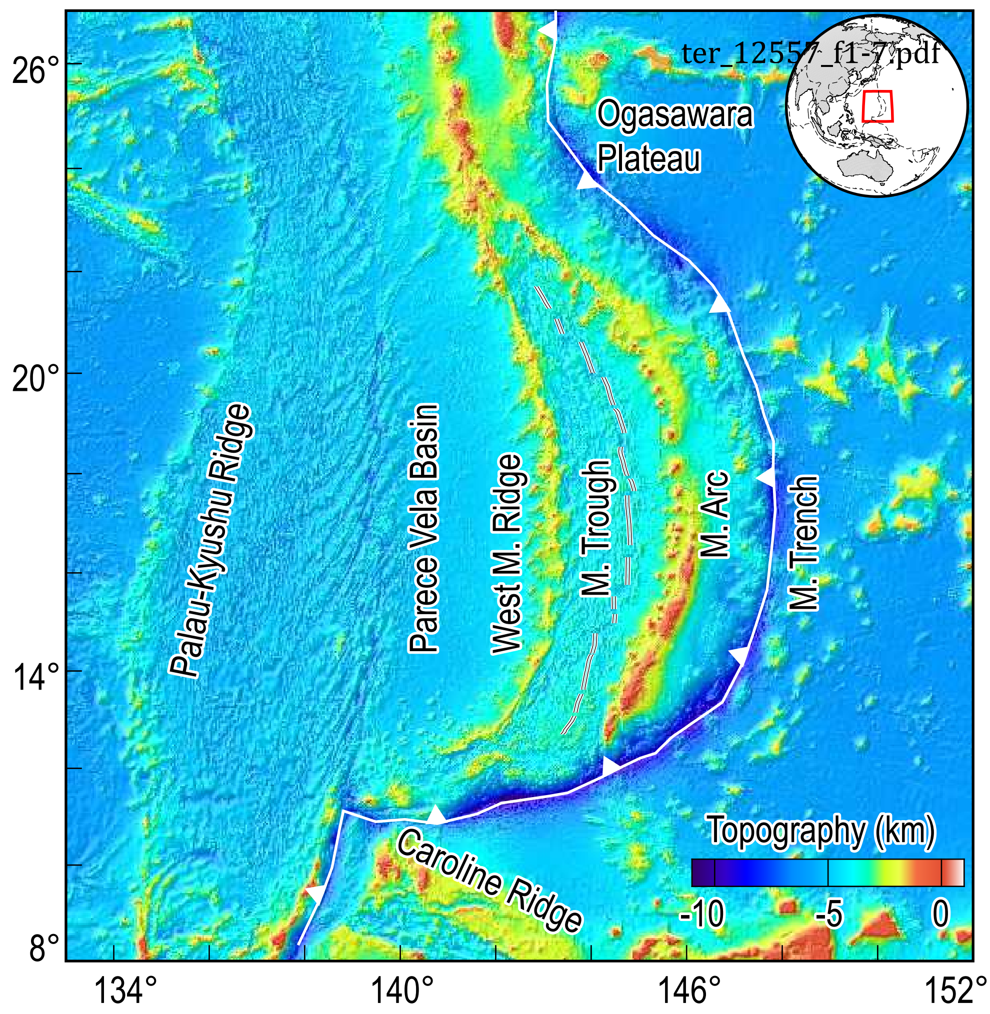
ter_12557_f1-7.pdf
Ogasawara
Plateau
Palau-Kyushu Ridge
Parece Vela Basin
West M. Ridge
M. Trough
M. Arc
M. Trench
Caroline Ridge
Topography (km)
-10
-5
0
26°
20°
14°
8°
134°
140°
146°
152°

Fig. 1

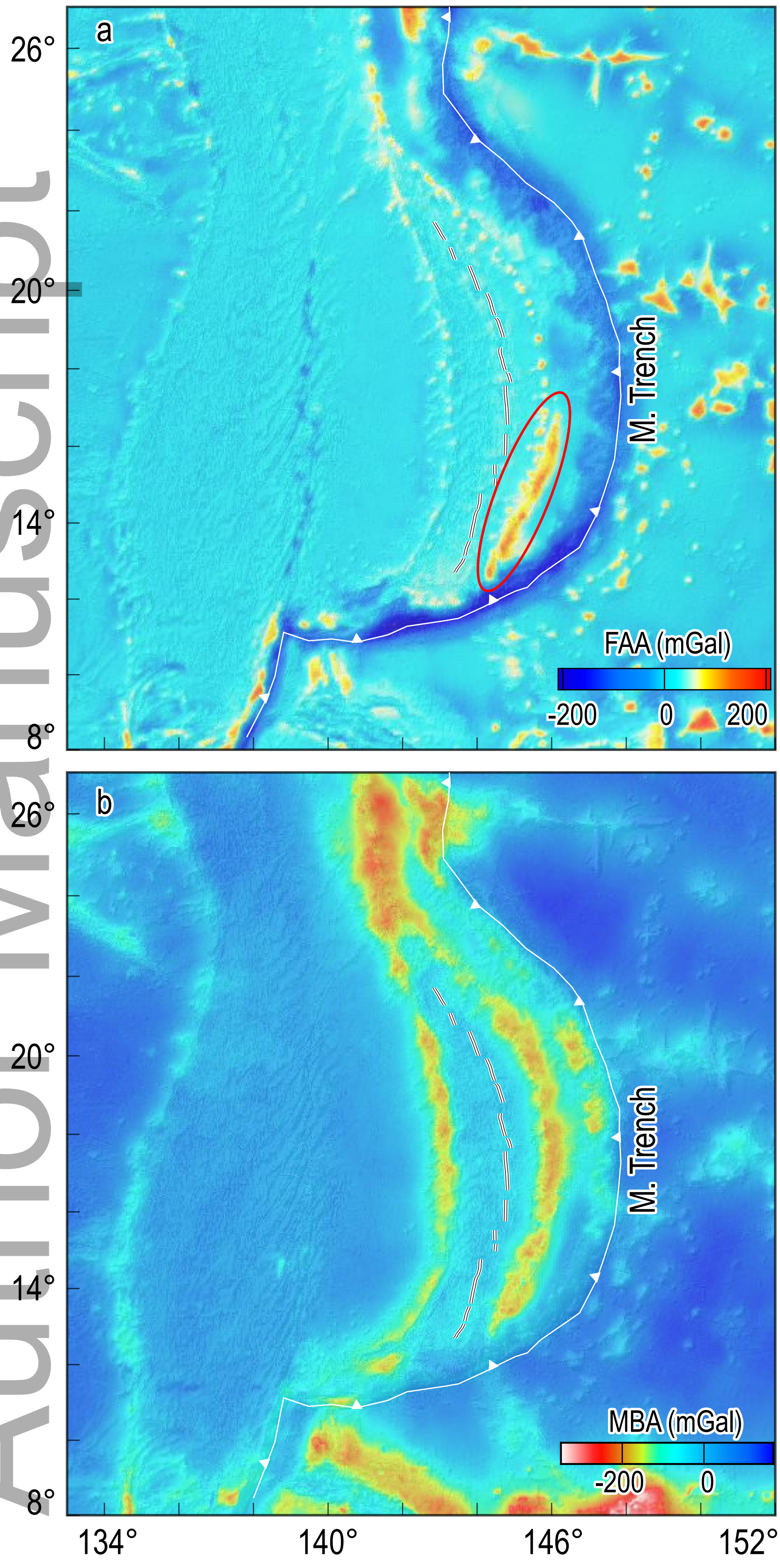

a
26°
20°
14°
8°
M. Trench
FAA (mGal)
-200
0
200
b
26°
20°
14°
8°
M. Trench
MBA (mGal)
-200
0
134°
140°
146°
152°

Fig. 2

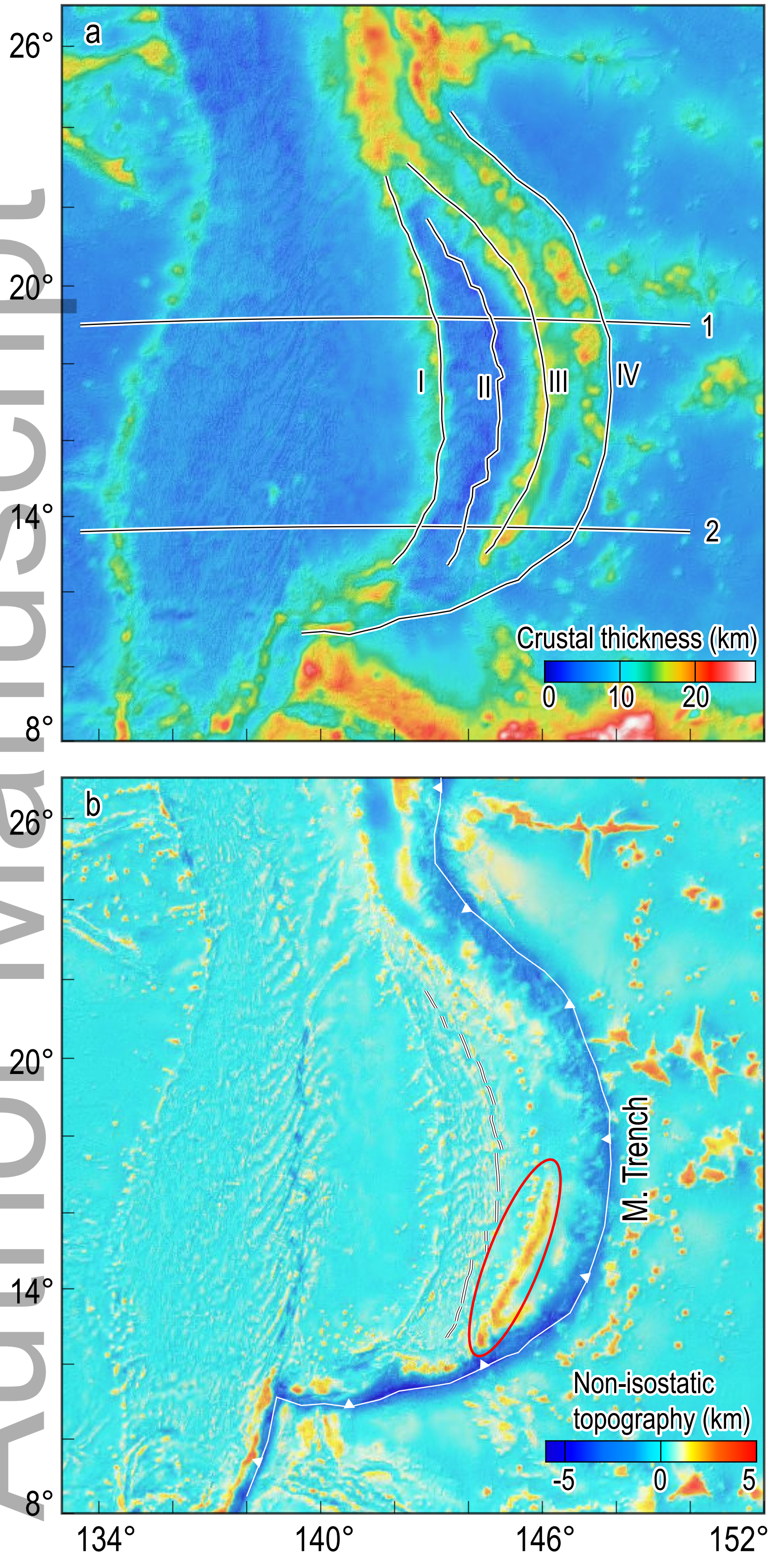
a
26°
20°
14°
8°
1
2
I
II
III
IV
Crustal thickness (km)
0
10
20
b
26°
20°
14°
8°
M. Trench
Non-isostatic topography (km)
-5
0
5
134°
140°
146°
152°

Fig. 3

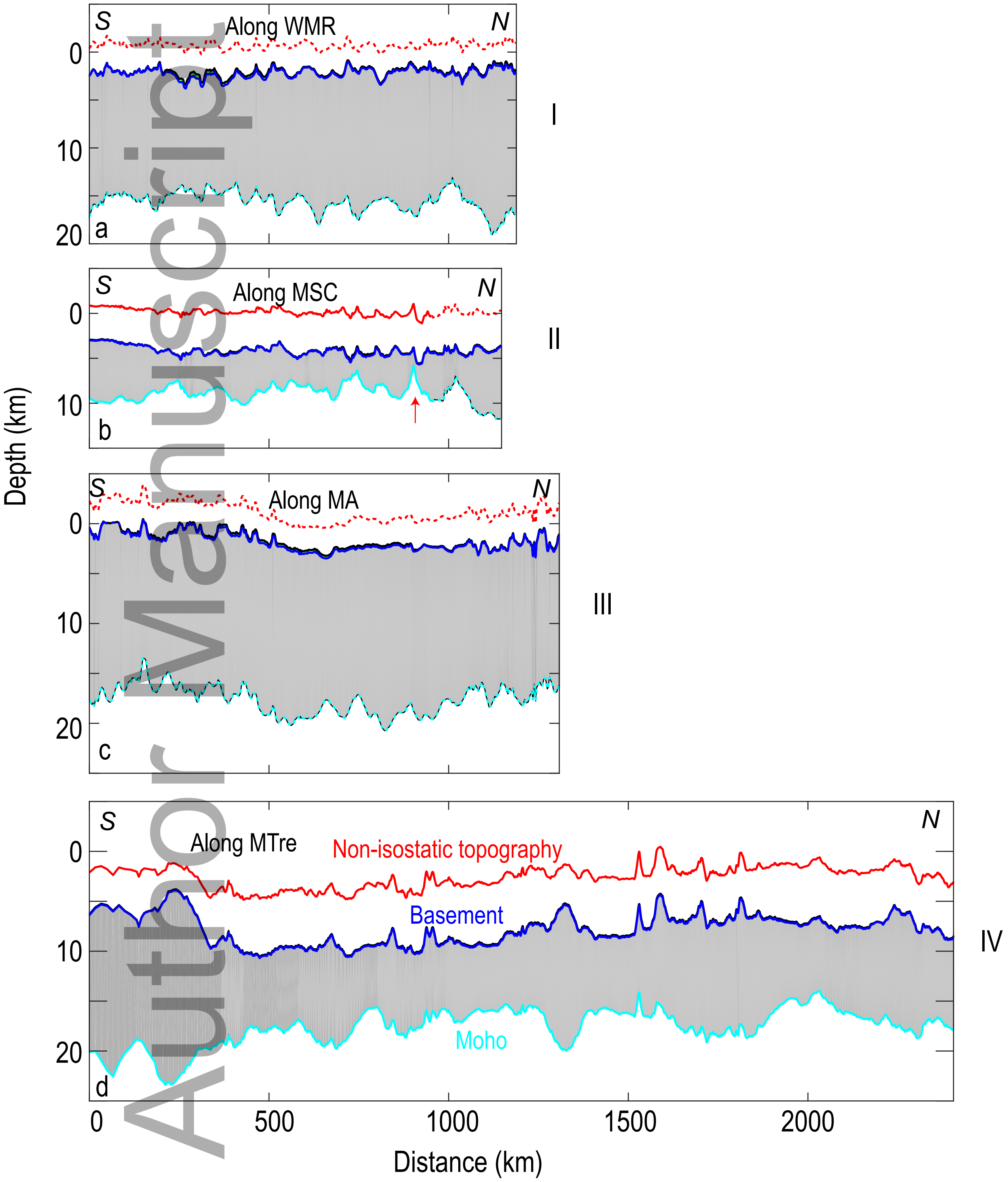

S
Along WMR
N
I
a
S
Along MSC
N
II
b
S
Along MA
N
III
c
S
Along MTre
Non-isostatic topography
N
Basement
IV
Moho
d
Depth (km)
Distance (km)
0
10
20
0
500
1000
1500
2000

Fig. 4

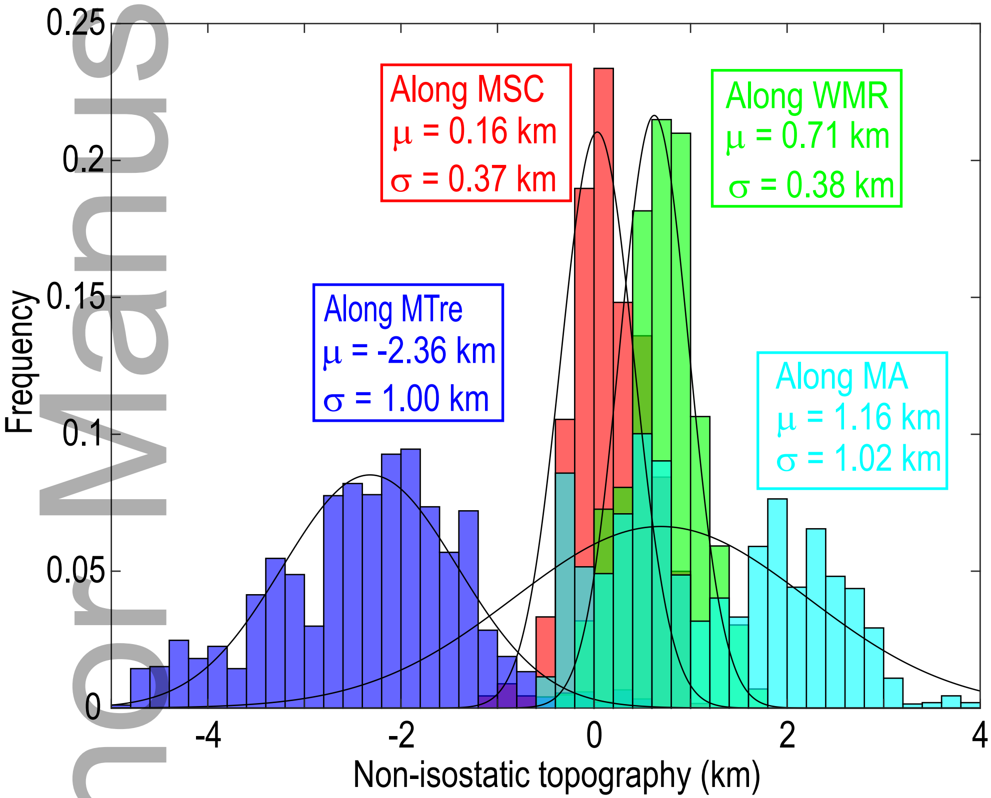
Along MSC
μ = 0.16 km
σ = 0.37 km
Along WMR
μ = 0.71 km
σ = 0.38 km
Along MTre
μ = -2.36 km
σ = 1.00 km
Along MA
μ = 1.16 km
σ = 1.02 km
Frequency
0.25
0.2
0.15
0.1
0.05
0
-4
-2
0
2
4
Non-isostatic topography (km)

Fig. 5

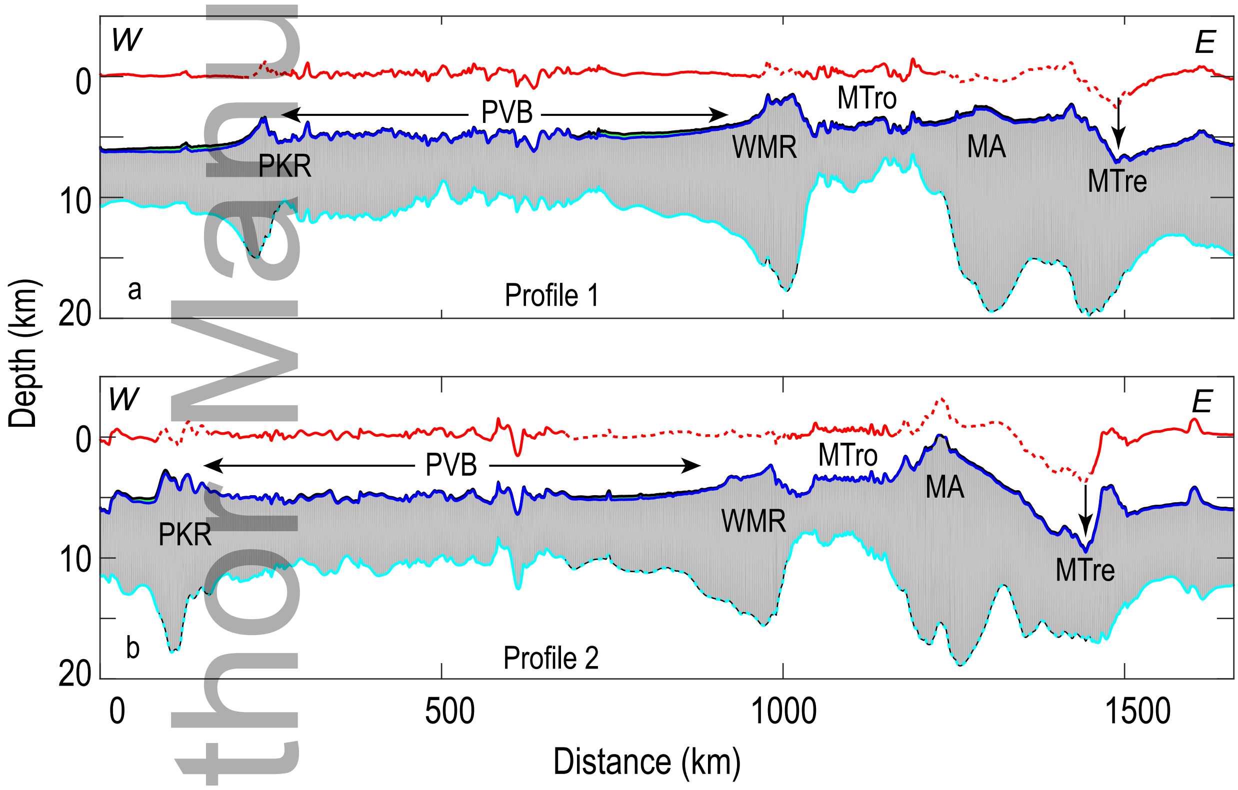
W
E
0
10
20
PVB
PKR
WMR
MTro
MA
MTre
a
Profile 1
Depth (km)
W
E
0
10
20
PVB
PKR
WMR
MTro
MA
MTre
b
Profile 2
0
500
1000
1500
Distance (km)

Fig. 6

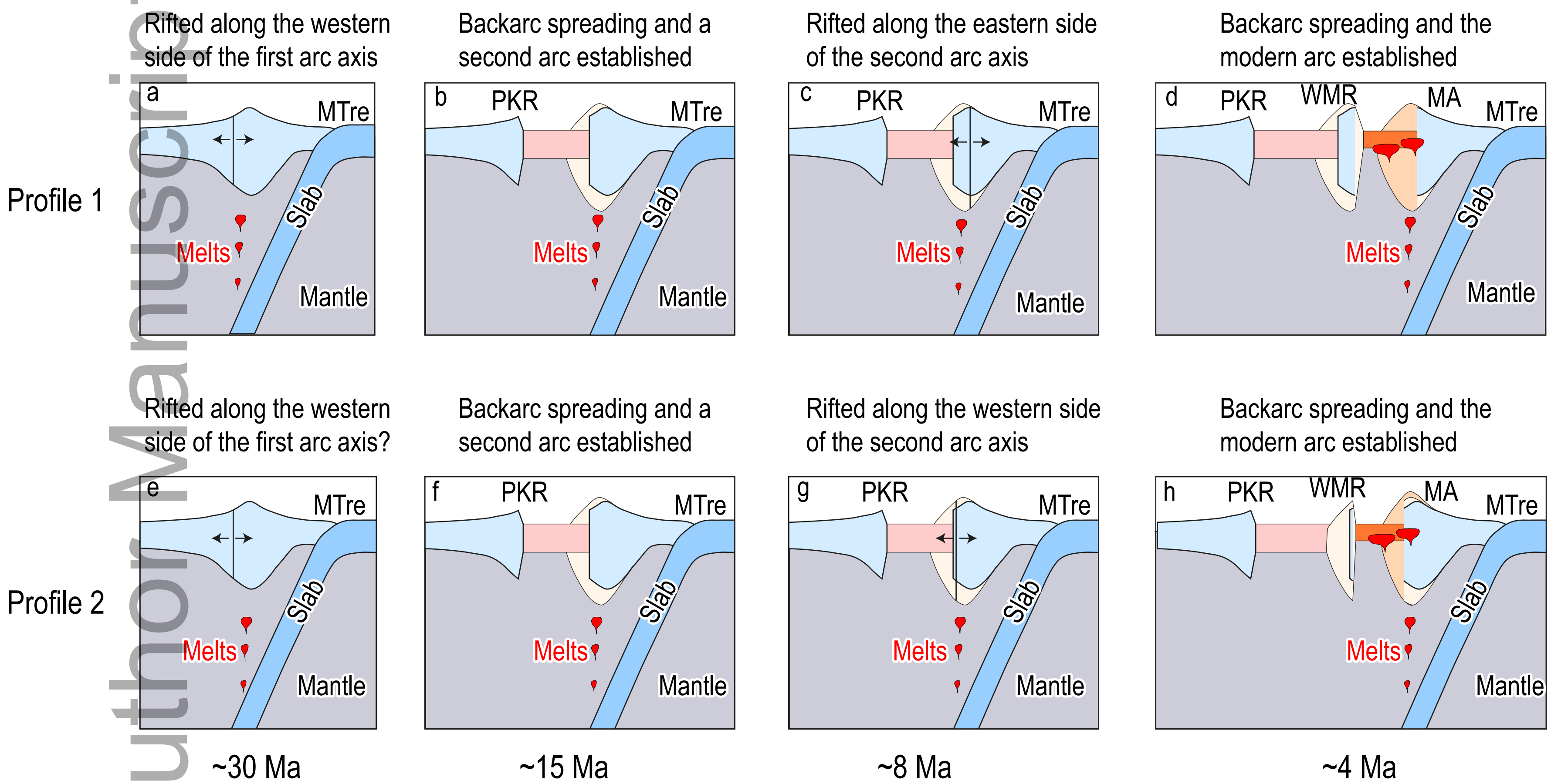

Rifted along the western side of the first arc axis
Backarc spreading and a second arc established
Rifted along the eastern side of the second arc axis
Backarc spreading and the modern arc established
Profile 1
a
b
c
d
PKR
WMR
MA
MTre
Slab
Melts
Mantle
Rifted along the western side of the first arc axis?
Backarc spreading and a second arc established
Rifted along the western side of the second arc axis
Backarc spreading and the modern arc established
Profile 2
e
f
g
h
~30 Ma
~15 Ma
~8 Ma
~4 Ma

Fig. 7